dynamic behaviors are discovered that are inconsistent with control of oxidized-reduced transitions by bromide ion alone, it does not seem to be useful to invoke other principles that can also explain some of the known facts.

The present paper has examined seemingly conflicting evidence about the rate of precipitation of AgBr and has considered the implications of that evidence for the mechanism of silver ion induced oscillations in the Belousov-Zhabotinsky system. Many of the same conclusions were reached by some of us[31] in a more general review of the control of bromate-driven oscillators.

Peter Ruoff also wishes to note that he has reservations as to the possibility that measurements with a silver wire electrode can provide any useful information concerning the initial processes during reaction of freshly mixed silver and bromide ions. His arguments will be developed in a separate paper.

Acknowledgment. The preparation of this paper was supported by Grants No. CHE-8717791 and CHE-8518879 from the National Science Foundation to R.M.N. and R.J.F., respectively, and by a grant from the Stiftung Volkswagenwerk to H.D.F.

Registry No. Ag^+, 14701-21-4.

(31) Ruoff, P.; Varga, M.; Körös, E. *Acc. Chem. Res.* **1988**, *21*, 326-332.

Pressure and Temperature Dependence of the Reaction $F + FSO_3 + M \rightarrow FSO_2OF + M$

A. E. Croce de Cobos, C. J. Cobos, and E. Castellano*

Instituto de Investigaciones Fisicoquímicas Teóricas y Aplicadas (INIFTA),† C. C. 16, Sucursal 4, (1900) La Plata, Argentina *(Received: March 15, 1988)*

The kinetics of the reaction $F + FSO_3 + M \rightarrow FSO_2OF + M$ (1) has been studied by using an ArF excimer laser flash photolysis/visible absorption technique to monitor the disappearance of FSO_3 radicals. He, N_2, and SF_6 were used as bath gases in pressures ranging from 5 to 600 Torr at 298 K; CF_4 was used in the same pressures between 298 and 378 K. Reaction 1 was found to be in the falloff region between second- and third-order kinetics. The following limiting high- and low-pressure recombination rate constants have been determined at 298 K: $k_{rec,\infty} = (7.6 \pm 1.0) \times 10^{-11}$ cm^3 molecule^{-1} s^{-1}, $k_{rec,0} = [He](4.1 \pm 0.5) \times 10^{-28}$, $[N_2](5.2 \pm 0.7) \times 10^{-28}$, $[CF_4](1.1 \pm 0.2) \times 10^{-27}$, and $[SF_6](1.3 \pm 0.2) \times 10^{-27}$ cm^3 molecule^{-1} s^{-1}. $k_{rec,\infty}$ and $k_{rec,0}$ showed a temperature dependence of $T^{0.23}$ and $T^{-3.1}$ (M = CF_4), respectively. With the $k_{rec,\infty}$ data and the known values of the high-pressure rate constant for FSO_2OF thermal decompositon, the equilibrium constant and the thermodynamical parameters of the system were obtained. An analysis of the $k_{rec,0}$ with respect to energy-transfer properties was performed. In terms of the canonical version of the statistical adiabatic channel model, the $k_{rec,\infty}$ values lead to $\alpha/\beta = 0.49$ for the ratio between the looseness and the Morse parameters. Specific rate constants derived from our experiments are also discussed.

Introduction

A knowledge of the kinetics of free-radical reactions is of major importance. In addition to the kinetic information itself, the study of free-radical reactions frequently provides the necessary data for the determination of their thermodynamic properties. In particular, dissociation-recombination reactions which involve the breaking or making of a simple bond can provide a specially searching test for theories of unimolecular reactions.

Although much is know about steady-state mechanistic kinetics studies of reactions in which the fluorosulfate radical FSO_3 is involved, very little has been performed under laser flash photolysis conditions. As a matter of fact, Schumacher and co-workers have extensively examined the kinetics and the mechanism of reactions involving the FSO_3 radical, e.g., the thermal reaction between FSO_2OF and NO_2[1] and of the dimer of the FSO_3 radical, $F_2S_2O_6$, with NO_2,[2] the photochemical reactions of FSO_2OF with both SO_3 and SO_2 at 254 nm,[3] the thermal reaction of F_2 with $F_2S_2O_6$,[4] and the thermal decomposition of FSO_2OF in the presence of SO_3[5] and Cl_2.[6] On the other hand, direct measurements for just the self-reaction of FSO_3 radicals have been reported.[7,8]

In spite of the detailed knowledge related to the vibrational,[9-12] rotational,[13] and electronic[14] spectroscopy of the ground ($^2A_2$)[9-14] and excited ($^2E(2)$)[9,13] states of this radical, direct kinetic measurements involving other FSO_3 radical reactions are still lacking.

Therefore, a systematic investigation of the reaction kinetics of FSO_3 radicals with other radicals and molecules is under way. An excimer laser flash photolysis/visible absorption study of the pressure (5-600 Torr), temperature (298-378 K), and bath gas (M = He, N_2, CF_4, and SF_6) dependences of reaction 1 is reported

$$F + FSO_3 + M \rightarrow FSO_2OF + M \qquad (1)$$

here. Our data have been combined with already reported results of the reverse of reaction 1[5,6] to determine the equilibrium constant and the thermodynamical parameters of the system. In addition to the experimental data, valuable insight on the theoretical aspects of atom-radical reactions is provided by this study. The factorized form of the low-pressure unimolecular reaction rate theory[15,16]

† Facultad de Ciencias Exactas, Universidad Nacional de La Plata.

(1) Gatti, R.; Schumacher, H. J. *Z. Phys. Chem. (Munich)* **1968**, *62*, 159.
(2) von Ellenrieder, G.; Schumacher, H. J. *Z. Phys Chem. (Munich)* **1968**, *59*, 157.
(3) Basualdo, W. H.; Schumacher, H. J. *Z. Phys. Chem. (Munich)* **1965**, *47*, 57.
(4) Castellano, E.; Schumacher, H. J. *Z. Phys. Chem. (Munich)* **1965**, *44*, 57.
(5) Czarnowski, J.; Castellano, E.; Schumacher, H. J. *Z. Phys. Chem. (Munich)* **1968**, *57*, 249.
(6) von Ellenrieder, G.; Schumacher, H. J. *Z. Phys. Chem. (Munich)* **1968**, *60*, 49.
(7) San Román, E.; Aramendía, P. F.; Schumacher, H. J. *An. Asoc. Quím. Argent.* **1982**, *70*, 887.
(8) Cobos, C. J.; Croce de Cobos, A. E.; Hippler, H.; Castellano, E., submitted for publication.
(9) King, G. W.; Warren, C. H. *J. Mol. Spectrosc.* **1969**, *32*, 121.
(10) Susuki, E. M.; Nibler, J. W.; Oakes, K. A.; Eggers, Jr., D. *J. Mol. Spectrosc.* **1975**, *58*, 201.
(11) Warren, C. H. *Chem. Phys. Lett.* **1979**, *68*, 407.
(12) Warren, C. H. *J. Mol. Spectrosc.* **1980**, *83*, 451.
(13) King, G. W.; Warren, C. H. *J. Mol. Spectrosc.* **1969**, *32*, 138.
(14) King, G. W.; Santry, D. P.; Warren, C. H. *J. Mol. Spectrosc.* **1969**, *32*, 108.
(15) Troe, J. *J. Chem. Phys.* **1977**, *66*, 4758.
(16) Troe, J. *J. Phys. Chem.* **1979**, *83*, 114.

0022-3654/89/2093-0274$01.50/0

and the canonical version of the statistical adiabatic channel model (SACM)[17] were employed for these calculations.

Experimental Section

The excimer laser flash photolysis/visible absorption setup has been described previously.[8] The reactants of reaction 1 were produced by 193-nm photolysis of fluorine fluorosulfonate (FSO_2OF) using an ArF excimer laser (Lambda Physik EMG 101 MSC). The temporal variation of FSO_3 radical concentration was resolved by monitoring their light absorption at 450 nm provided by a 150-W xenon arc lamp (Hanovia 901C-1). The reaction cell was contained in an electrically heatable heavy aluminum housing. A calibrated chromel–alumel thermocouple served to measure the temperature of the reaction mixtures. After passage through the reaction cell, the probed light was focused on the entrance slit of a prism monochromator (Zeiss MM12). A photomultiplier (RCA 1P28) and a digital oscilloscope (Nicolet 2090) served for signal detection and recording, respectively. The laser pulse energy incident on the photolysis cell was measured with a joulemeter (Gentec). A pulse laser fluence of about 60 mJ cm^{-2} was employed in these single-shot experiments.

The cell was evacuated and filled via a conventional vacuum line, and the pressure measurements were performed using a quartz spiral gauge.

FSO_2OF was prepared by photolyzing a mixture of F_2 and SO_3 in a Pyrex photochemical reactor with a Hanau Q700 mercury arc lamp.[18] The reaction products (FSO_2OF and $F_2S_2O_6$) were condensed at 195 K. The volatile fraction at 163 K resulting from trap-to-trap distillations consisted of FSO_2OF. The FSO_2OF purity was checked by IR spectrophotometry. The bath gases used have the following stated minimum purities: He, 99.999% (Union Carbide); N_2, 99.99% (La Oxigena); CF_4, 99.7% (Matheson); and SF_6, 99.999% (Matheson).

Results and Discussion

The FSO_2OF molecule and the FSO_3 radical absorb radiation in different regions of the UV–visible spectra. The FSO_2OF presents a continuous absorption below about 420 nm with increasing intensity as the wavelength decreases.[19] At the photolysis wavelength, 193 nm, its absorption cross section is $\sigma(FSO_2OF) = (1.57 \pm 0.07) \times 10^{-18}$ cm^2 $molecule^{-1}$.[19] On the other hand, the FSO_3 radical has a strong absorption band between 550 and 380 nm.[14] In a previous work[8] we have measured the absorbance at 450 nm of $F_2S_2O_6 \rightleftharpoons 2FSO_3$ equilibrium mixtures over the temperature range 310–334 K. Since the equilibrium constant for this system is known,[8,20,21] an absorbance vs $[FSO_3]$ plot, where $[FSO_3] = (K_c[F_2S_2O_6])^{1/2}$, yields the absorption cross section of the FSO_3 radical, $\sigma(FSO_3) = (3.64 \pm 0.32) \times 10^{-18}$ cm^2 $molecule^{-1}$ at the monitoring wavelength of 450 nm. The error estimates quoted for our absorption cross section measurements represent two standard deviations. At the same wavelength $\sigma(FSO_2OF)$ is $< 1 \times 10^{-23}$ cm^2 $molecule^{-1}$.[19]

Electron paramagnetic resonance studies of UV-irradiated FSO_2OF in a low-temperature matrix showed the production of FSO_3 radicals.[22] In addition, the gas-phase photolysis of FSO_2OF at 254 nm in the presence of SO_3 is consistent with a unitary quantum yield of FSO_3 radicals.[3] From the concentration of FSO_3 initially generated and the number of 193-nm photons absorbed by FSO_2OF during the laser pulse, a primary quantum yield of 1.09 ± 0.15 FSO_3 radicals per quantum is obtained. Further details about the quantum yield measurements are given elsewhere.[19] Therefore, F atoms and FSO_3 radicals are exclusively generated in the 193-nm photolysis of FSO_2OF, FSO_3 radicals being probed by the analytical beam. FSO_3 radicals produced in the primary process could react in two ways, either by reaction 1 or by the self-reaction

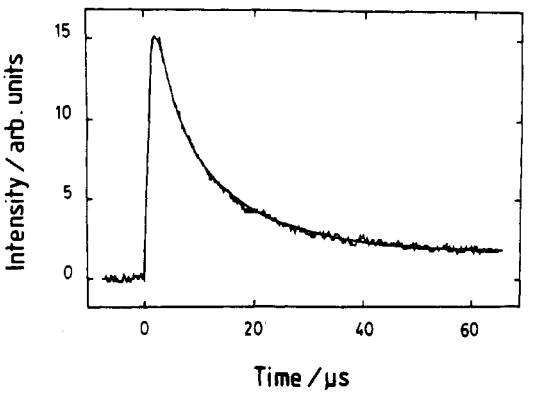

Figure 1. Typical FSO_3 temporal profiles observed at 450 nm following 193-nm photolysis of 1.3 Torr of FSO_2OF and 21.8 Torr of CF_4 at 298 K. The fit yields a second-order rate constant for reaction 1 of 3.6×10^{-11} cm^3 $molecule^{-1}$ s^{-1}.

$$FSO_3 + FSO_3 \rightarrow F_2S_2O_6 \quad (2)$$

The limiting high-pressure rate constant of reaction 2 has been measured[8] and, as will be shown below, is at least a factor of 300 smaller than the rate constants of reaction 1. Reaction 2 could then be ignored unless the concentration of F atoms was depleted by reactions faster than (1). For several reasons the consumption of F atoms by reactions other than (1) is also unimportant and can be ruled out. Actually, in addition to reaction 1 F atoms can disappear through reactions

$$F + FSO_2OF \rightarrow F_2 + FSO_3 \quad (3)$$

$$F + F + M \rightarrow F_2 + M \quad (4)$$

$$F \rightarrow \text{diffusive loss} \quad (5)$$

Reaction 3 has a relatively high activation energy, $E_3 \simeq 9.7$ kcal mol^{-1}, as can be calculated from $E_3 = E_{-3} + D(FSO_2O\text{–}F) - 2\Delta H^\circ_{298}(F)$ by taking the activation energy of the reverse of process 3, $E_{-3} = 14.7$ kcal mol^{-1},[4] the limiting high-pressure activation energy of the thermal FSO_2OF dissociation $E_{-1,\infty} \simeq D(FSO_2O\text{–}F) = 32.8$ kcal mol^{-1},[5,6] and $\Delta H^\circ_{298}(F) = 18.9$ kcal mol^{-1}.[23] Therefore, in our experimental conditions reaction 3 must be very slow. Termolecular reaction 4 is also a slow process.[24] The diffusion of F atoms away from the field of view of the detector is also a slow process when compared with the FSO_3 radical decay time (less than 350 μs for experiments with 5 Torr of He). Therefore, it must be concluded that the observed FSO_3 radical decay corresponds to reaction 1.

The kinetics of reaction 1 is described by a second-order rate law which, employing Beer's law, has the solution

$$\frac{1}{\ln (I_0/I(t))} = \frac{k_{rec}t}{\sigma l} + \frac{1}{\ln (I_0/I')} \quad (6)$$

where σ is the FSO_3 absorption cross section at 450 nm, l the absorption path length, I_0 the incident light intensity, $I(t)$ the transmitted light intensity at time t, and I' the transmitted light intensity immediately after the laser pulse. Analysis of the second-order kinetic decay plots [$1/\ln (I_0/I(t))$ vs time] yields the bimolecular rate constants k_{rec} of reaction 1. A typical experimental decay profile and its fit to eq 6 are represented in Figure 1.

Reaction 1 was studied as a function of total pressure (5–600 Torr), temperature (298–378 K), and diluent gases (M = He, N_2, CF_4, and SF_6). Similar results were obtained with FSO_2OF pressures ranging between 0.2 and 5 Torr. A spectral resolution $\Delta\lambda$(fwhm) = 3.3 nm was used in our time-resolved experiments.

(17) Troe, J. *J. Chem. Phys.* **1981**, *75*, 226.
(18) Gambaruto, M.; Sicre, J. E.; Schumacher, H. J. *J. Fluorine Chem.* **1975**, *5*, 175.
(19) Croce de Cobos, A. E., to be published.
(20) Dudley, F. B.; Cady, G. H. *J. Am. Chem. Soc.* **1963**, *85*, 3375.
(21) Castellano, E.; Gatti, R.; Sicre, J. E.; Schumacher, H. J. *Z. Phys. Chem. (Munich)* **1964**, *42*, 174.
(22) Neumayr, F.; Vanderkooi, Jr., N. *Inorg. Chem.* **1965**, *4*, 1234.
(23) *JANAF Thermochemical Tables*, 2nd ed.; *Natl. Stand. Ref. Data Ser. (U.S., Natl. Bur. Stand.)* **1971**, *37*.
(24) Kerr, J. A.; Moss, S. J. *CRC Handbook of Bimolecular and Termolecular Gas Reactions*; CRC Press: Boca Raton, FL, 1981; Vol. II.

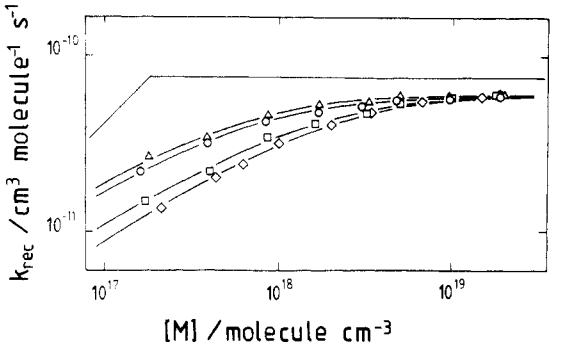

Figure 2. Pressure dependence of the rate constants for reaction 1 at 298 K: ◇, M = He; □, M = N_2; ○, M = CF_4; △, M = SF_6. Solid lines are curve fits to the data using the falloff equation (eq 7 and 8). The high-pressure rate constant and the low-pressure rate constant for M = He are also shown.

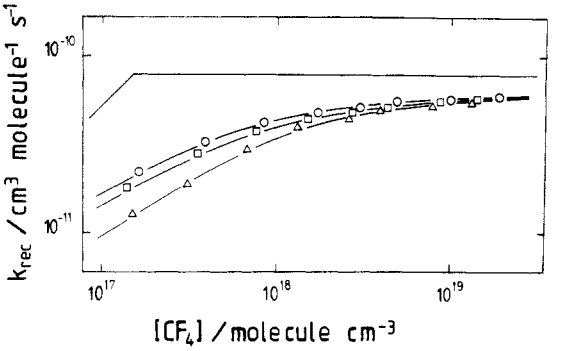

Figure 3. Temperature and pressure dependences of the rate constants for reaction 1 for M = CF_4: ○, T = 298 K; □, T = 339 K; △, T = 378 K. Solid lines are curve fits to the data using the falloff equation (eq 7 and 8). The high-pressure and low-pressure rate constants at 378 K are also shown.

Figure 2 shows how the second-order rate constants at 298 K derived from the experiments vary with the total concentration. The rate constants change by a factor of 4.2 for M = He, 3.7 for M = N_2, 2.7 for M = CF_4, and 2.3 for M = SF_6, over the pressure range investigated. Figure 3 shows the temperature dependence of the experiments with diluent CF_4. In this case, the rate constants change by a factor of 1.7 between 298 and 378 K at the lowest pressure investigated while at the higher values only a slight temperature dependence is observed. Each point in Figures 2 and 3 represents an average of four to eight experiments. Since even at the highest bath gas concentrations the rate constants show slow increasing values, it is evident that, although very close to the high-pressure limit, our experiments still lie in the falloff regime between second- and third-order kinetics. A fit of the experimental data for each third-body gas at each temperature to falloff curves representing the pressure dependence of k_{rec} has to be made to obtain the limiting high- and low-pressure recombination rate constants $k_{rec,\infty}$ and $k_{rec,0}$.

Analysis of the Falloff Curves. The most commonly used technique currently applied in the analysis of the falloff curves is the Troe factorized method[16]

$$k_{rec} = k_{rec,\infty} F^{LH}(\gamma)\, F^{SC}(\gamma,S_K)\, F^{WC}(\gamma,S_K,\beta_c) \qquad (7)$$

All the F factors depend on the ratio $\gamma = k_{rec,0}/k_{rec,\infty}$ as a dimensionless scale. The Lindemann–Hinshelwood factor $F^{LH}(\gamma) = 1/(1 + 1/\gamma)$ is a switching function that describes the transition of k_{rec} from $k_{rec,0}$ to $k_{rec,\infty}$. F^{SC} allows for broadening due to the spread in the values of the energy-dependent specific rate constants of energized adducts, and F^{WC} accounts for weak collision effects via the collision efficiency of the diluent gas β_c. The parameter S_K is related to the internal energy of the activated complex by the following relationship

$$S_K = 1 + T\frac{\partial \ln Q^{\ddagger}}{\partial T} \qquad (8)$$

TABLE I: Limiting High- and Low-Pressure Rate Constants for Reaction 1

T/K	M	$k_{rec,\infty}$/cm^3 molecule^{-1} s^{-1}	$k_{rec,0}$/cm^3 molecule^{-1} s^{-1}
298	He	(8.1 ± 0.8) × 10^{-11}	(4.1 ± 0.5) × 10^{-28}
298	N_2	(7.7 ± 0.8) × 10^{-11}	(5.2 ± 0.7) × 10^{-28}
298	SF_6	(7.2 ± 0.8) × 10^{-11}	(1.3 ± 0.2) × 10^{-27}
298	CF_4	(7.2 ± 0.8) × 10^{-11}	(1.1 ± 0.2) × 10^{-27}
339	CF_4	(7.4 ± 0.8) × 10^{-11}	(7.5 ± 0.9) × 10^{-28}
378	CF_4	(7.6 ± 0.8) × 10^{-11}	(5.3 ± 0.6) × 10^{-28}

where $Q^{\ddagger}$ is the rotation–vibration partition function of the activated complex.[25] In ref 26 and 27, S_K was evaluated by employing $Q^{\ddagger}$ as given by the canonical version of the statistical adiabatic channel model.[17] Nevertheless, in the present study S_K was derived from the temperature dependence of the extrapolated $k_{rec,\infty}$ values.[28] In order to deduce an expression for S_K, the results were represented in the form

$$k_{rec,\infty} = A_\infty (T/300)^{n_\infty} \qquad (9)$$

and the following equation was used to obtain $Q^{\ddagger}$[17]

$$k_{rec,\infty} = \frac{kT}{h}\left(\frac{h^2}{2\pi\mu kT}\right)^{3/2} \frac{Q_e(FSO_2OF)}{Q_e(F)\, Q_e(FSO_3)} \frac{Q^{\ddagger}}{Q_{vib}(FSO_3)\, Q_{rot}(FSO_3)} \qquad (10)$$

Here μ denotes the reduced mass of the reaction partners, $Q_e(i)$ denotes the electronic partition functions of reactants and products, and Q_{vib} and Q_{rot} denote the vibrational and the rotational partition functions of the FSO_3 radical, respectively. Taking into account eq 7 and 10 and assuming classical rotational partition functions for the FSO_3 radical, we derived the expression

$$S_K = n_\infty + 3 + 2\frac{\frac{\epsilon_1}{kT}\exp\left(-\frac{\epsilon_1}{kT}\right)}{4 + 2\exp\left(-\frac{\epsilon_1}{kT}\right)} + T\frac{\partial \ln Q_{vib}(FSO_3)}{\partial T} \qquad (11)$$

where ϵ_1 = 404 cm^{-1} [23] is the lower electronically excited level of F atoms. Assuming β_c = 0.5 for CF_4, the fit of the experimental data with eq 7 and 8 has been realized, wherein an initial value of n_∞ = 0 has been chosen as a first approximation.[28] A nonlinear least-squares fit to the measured bimolecular rate constants at 298, 339, and 378 K (Figure 3) yielded a set of $k_{rec,\infty}$ values. These results are fitted with eq 9 in order to obtain a new n_∞ value, which is used for a further evaluation of the limiting rate constants. The iterative procedure was repeated until convergence of n_∞. The final results are given in Table I, where the error limits quoted for the rate constants represent one standard deviation plus the uncertainty of the falloff extrapolations. The temperature dependence of the experimental results can be represented by the following equations

$$k_{rec,\infty} = 7.2 \times 10^{-11}(T/300)^{0.23} \text{ cm}^3 \text{ molecule}^{-1} \text{ s}^{-1} \qquad (12)$$

$$k_{rec,0} = [CF_4](1.1 \times 10^{-27})(T/300)^{-3.1} \text{ cm}^3 \text{ molecule}^{-1} \text{ s}^{-1} \qquad (13)$$

The limiting rate constants for the bath gases He, N_2, and SF_6 at 298 K have been obtained by extrapolation, taking n_∞ = 0.23 (S_K = 4.83). Table I shows the best fit for $k_{rec,\infty}$ and $k_{rec,0}$. Such high $k_{rec,\infty}$ values are typical for atom–radical reactions in the high-pressure regime.[24,29,30] Taking the statistical spread of the

(25) Gardiner, Jr., W. C.; Troe, J. In *Combustion Chemistry*; Gardiner, Jr., W. C., Ed.; Springer-Verlag: New York, 1984.
(26) Cobos, C. J.; Hippler, H.; Troe, J. *J. Phys. Chem.* **1985**, *89*, 342.
(27) Cobos, C. J.; Hippler, H.; Luther, K.; Ravishankara, A. R.; Troe, J. *J. Phys. Chem.* **1985**, *89*, 4332.
(28) Keiffer, M.; Pilling, M. J.; Smith, M. J. C. *J. Phys. Chem.* **1987**, *91*, 6028.
(29) Baulch, D. L.; Cox, R. A.; Hampson, R. F.; Kerr, J. A.; Troe, J.; Watson, R. T. *J. Phys. Chem. Ref. Data* **1984**, *13*, 1259.

results into account, the average value at 298 K, $k_{rec,\infty}$ = (7.6 ± 1.0) × 10^{-11} cm^3 $molecule^{-1}$ s^{-1}, and the following expression for the temperature dependence of the rate constants over the range 298–378 K

$$k_{rec,\infty} = 7.6 \times 10^{-11}(T/300)^{0.23} \text{ cm}^3 \text{ molecule}^{-1} \text{ s}^{-1} \quad (14)$$

has been obtained. The weak temperature dependence found here for $k_{rec,\infty}$ is typical for this kind of reaction.[24,29,30] The $k_{rec,0}$ values derived from our experiments are appreciably higher than those normally reported in the literature. Nevertheless the temperature dependence of $k_{rec,0}/[CF_4]$ is normal.[24,29,30]

Evaluation of the Equilibrium Constant and Thermochemistry of the System. Our temperature-dependent $k_{rec,\infty}$ values can be combined with the limiting high-pressure dissociation rate constants $k_{diss,\infty}$, resulting from the thermal dissociation of FSO_2OF,[5,6] to estimate the equilibrium constant $K_c = k_{diss,\infty}/k_{rec,\infty}$. The experimental falloff curves reported at 364, 374, 384, and 394 K by Schumacher and co-workers[5,6] were fitted as above, resulting in the Arrhenius expression $k_{diss,\infty} = 9.4 \times 10^{14} \exp[-(32.8 \pm 0.7)/RT]$ s^{-1}. This equation agrees very well with the one obtained from the extrapolated $k_{diss,\infty}$ values assigned in ref 5 and 6, $k_{diss,\infty} = 9.9 \times 10^{14} \exp[-(32.8 \pm 1.1)/RT]$ s^{-1}. The recombination data (298–378 K) together with the dissociation results evaluated here (364–394 K) lead to individual $k_{diss,\infty}/k_{rec,\infty}$ ratios. In this way, the following expression over the temperature range 298–394 K is obtained

$$K_c = 9.0 \times 10^{24} \exp(-16408/T) \text{ molecules cm}^{-3} \quad (15)$$

In order to derive the standard enthalpy, $\Delta H°_{298}$, and the standard entropy, $\Delta S°_{298}$, changes of the reverse of reaction 1, the K_c values were expressed in units of partial pressure, $K_p = K_c RT$. A plot of $\ln K_p + (\Delta C_p/R)[\ln(298/T) + (T - 298)/T]$ against $1/T$ allows one to determine $\Delta H°_{298}$ and $\Delta S°_{298}$ from the slope and intercept to $1/T = 0$, respectively. Already reported values of vibrational frequencies of FSO_2OF[31] and FSO_3[9-12] were used to calculate the change in the molar heat capacities, ΔC_p. This treatment leads to the following values: $\Delta H°_{298}$ = 33.1 ± 0.9 kcal mol^{-1} and $\Delta S°_{298}$ = 27.2 ± 1.2 cal mol^{-1} K^{-1}. The standard enthalpy and entropy changes of reactions 1 and 2 can be easily combined to derive the standard enthalpy and entropy of FSO_2OF. In this way, the following relationships are deduced

$$\Delta H_f°_{298}(FSO_2OF) = \Delta H_f°_{298}(F) + \tfrac{1}{2}[\Delta H_f°_{298}(F_2S_2O_6) - \Delta H°_{298}(2)] + \Delta H°_{298}(1) \quad (16)$$

$$S°_{298}(FSO_2OF) = S°_{298}(F) + \tfrac{1}{2}[S°_{298}(F_2S_2O_6) - \Delta S°_{298}(2)] + \Delta S°_{298}(1) \quad (17)$$

The standard enthalpy of formation of FSO_2OF is estimated as $\Delta H_f°_{298}(FSO_2OF)$ = −141.2 ± 2.0 kcal mol^{-1} employing $\Delta H_f°_{298}(F)$ = 18.9 ± 0.4 kcal mol^{-1},[23] $\Delta H_f°_{298}(F_2S_2O_6)$ = −276 ± 2 kcal mol^{-1},[32] and the standard enthalpy changes of reactions 1 and 2, $\Delta H°_{298}(1)$ = −33.1 ± 0.9 kcal mol^{-1} and $\Delta H°_{298}(2)$ = −22.1 ± 0.7 kcal mol^{-1},[8] respectively. Similarly, the standard entropy of FSO_2OF, $S°_{298}(FSO_2OF)$ = 80.3 ± 2.2 cal mol^{-1} K^{-1}, is obtained by replacing in eq 17 the values $S°_{298}(F)$ = 37.9 cal mol^{-1} K^{-1},[23] $S°_{298}(F_2S_2O_6)$ = 101 ± 2 cal mol^{-1} K^{-1},[32] $\Delta S°_{298}(1)$ = −27.2 ± 1.2 cal mol^{-1} K^{-1}, and $\Delta S°_{298}(2)$ = −38.2 ± 1.0 cal mol^{-1} K^{-1}.[8] No reported literature values are available for the comparison with our $\Delta H_f°_{298}(FSO_2OF)$ and $S°_{298}(FSO_2OF)$.

Analysis of the Limiting High-Pressure Rate Constants. We have interpreted the experimental $k_{rec,\infty}$ values in terms of the canonical version of the statistical adiabatic channel model.[17] The SACM provides a useful method to both determine $k_{rec,\infty}$ and systematize the essential features affecting these rate constants.[33]

According to the SACM, $k_{rec,\infty}$ is given, via detailed balance, by the following expression

$$k_{rec,\infty} = \frac{1}{K_c}\frac{kT}{h}\frac{Q^*_{cent}F^*_{AM}Q^*_mQ^*_j}{\sigma^*Q_{vib}Q_{rot}}\exp\left(-\frac{\Delta H°_0 + \Delta E^*_{0Z}}{kT}\right) \quad (18)$$

In this equation Q^*_{cent} denotes the centrifugal pseudopartition function, F^*_{AM} is an angular momentum coupling correction factor, σ^* is an effective symmetry number, Q^*_j is the pseudopartition function of the conserved oscillators of FSO_2OF, and Q^*_m is the product of the pseudopartition functions of the disappearing oscillators (these transitional modes are the torsion and the bending of the FSO_2–O–F bonds) and the pseudopartition function that accounts for the transformation between the appropriate rotational constants of FSO_2OF and FSO_3. Q_{vib} and Q_{rot} are vibrational and rotational partition functions of FSO_2OF, and K_c is the equilibrium constant given by eq 15. The threshold energy is essentially the FSO_2O–F bond dissociation energy at 0 K, $\Delta H°_0$, because the reaction has a very small adiabatic zero-point barrier at the lowest reaction channel ΔE^*_{0Z}. The value $\Delta H°_0$ = 32.4 kcal mol^{-1} was obtained from $\Delta H°_{298}$ and the vibrational frequencies of FSO_2OF[31] and FSO_3.[9-12] The quantities denoted by an asterisk depend on the potential energy surface of the reaction. In the SACM the variation of the electronic energy along the reaction coordinate q is approached with a Morse potential (with a parameter β = 3.0 $Å^{-1}$ as calculated using the O–F stretching force constant of CF_3OF[34]). Besides, the transformation from reactant to product eigenvalues is described by simple exponential switching functions of the form $S(q) = \exp[-\alpha(q - q_e)]$ with global looseness parameters α. The room-temperature value $k_{rec,\infty}$ = 7.6 × 10^{-11} cm^3 $molecule^{-1}$ s^{-1} was reproduced employing a ratio α/β = 0.49. This value agrees very well with the value used to fit numerous single-bond dissociation–recombination reactions $\langle\alpha/\beta\rangle$ = 0.46 ± 0.09.[33] The observed near constancy of α/β is supported by recent ab initio calculations.[35] It is interesting to note that by using the reported average value $\langle\alpha/\beta\rangle$ = 0.46, a $k_{rec,\infty}$ = 5.5 × 10^{-11} cm^3 $molecule^{-1}$ s^{-1} is predicted in very good agreement with the experimental result. The derived α/β = 0.49 was then employed to calculate the temperature dependence of $k_{rec,\infty}$. In this way, we obtain

$$k_{rec,\infty} = 7.6 \times 10^{-11}(T/300)^{0.15} \text{ cm}^3 \text{ molecule}^{-1} \text{ s}^{-1} \quad (19)$$

over the temperature range 300–400 K. This expression compares remarkably well with the value obtained from the experimental data (eq 12). The decrease of $k_{rec,\infty}$ from the value corresponding to the phase space limiting high-pressure rate constant $k_{rec,\infty}$(PSL) is accounted for by the rigidity factor $f_{rigid} = k_{rec,\infty}/k_{rec,\infty}$(PSL).[33] This factor takes explicitly into account the contraction of the available phase space of the reaction due mainly to the contribution of the internal degrees of freedom orthogonal to the reaction coordinate.[36] $k_{rec,\infty}$(PSL) is simply obtained by evaluation of eq 18 with $\alpha/\beta \to \infty$. In this way we calculate between 300 and 400 K an almost constant $f_{rigid} \simeq 0.19$. This value of f_{rigid} is consistent with those normaly found for atom–polyatomic radical recombination reactions.[33]

Collisional Energy Transfer of Highly Excited FSO_2OF. Falloff behavior for dissociation–recombination reactions depends on parameters that characterize collisions between the reactants and third-body gases. The differences observed in the falloff curves shown in Figures 2 and 3 are accounted for by the differences in the collisional-energy-transfer rate constants and by the average amount of the energy transferred in both activating and deactivating collisions between the energized FSO_2OF adduct and the bath gas M, $\langle\Delta E\rangle$. Conventionally, the collisional-energy-transfer rate constants are approached by Lennard-Jones collision frequencies Z_{LJ}.[15] $\langle\Delta E\rangle$ is related to the collision efficiency β_c. The magnitude of β_c can be evaluated from the ratio of the measured

(30) DeMore, W. B.; Margitan, J. J.; Molina, M. J.; Watson, R. T.; Hampson, R. F.; Kurylo, M. J.; Howard, C. J.; Ravishankara, A. R. "Chemical Kinetics and Photochemical Data for Use in Stratospheric Modelling", Evaluation No. 7, JPL Publication 85-37, 1985.
(31) Qureski, A. M.; Levchuk, L. E.; Aubke, F. *Can. J. Chem.* **1971**, *49*, 2544.
(32) Benson, S. W. *Chem. Rev.* **1978**, *78*, 23.
(33) Cobos, C. J.; Troe, J. *J. Chem. Phys.* **1985**, *83*, 1010.
(34) Wilt, P. M.; Jones, E. A. *J. Inorg. Nucl. Chem.* **1968**, *30*, 2933.
(35) Wolf, R. J.; Bathia, D. S.; Hase, W. L. *Chem. Phys. Lett.* **1986**, *132*, 493.
(36) Cobos, C. J. *J. Chem. Phys.* **1986**, *85*, 5644.

TABLE II: Bath Gas Collision Efficiencies and Average Energies Transferred per Collision

			$-\langle\Delta E\rangle$/cm^{-1}					
					CS_2[c]		azulene[d]	
T/K	M	β_c	exponential[a]	stepladder[b]	E_{exc} = 10000	E_{exc} = 36000	E_{exc} = 17500	E_{exc} = 30600
298	He	0.11	40	34	13	100	78	79
298	N_2	0.19	82	65	6.8	72	185	198
298	SF_6	0.50	414	235	130	490	644	720
298	CF_4	0.46	346	208	56	1120	390	450
339	CF_4	0.45	387	235				
378	CF_4	0.44	422	260				

[a] Exponential model (eq 21). [b] Stepladder model (eq 22 and 23). [c] From direct measurements of excited CS_2 at the given excitation energies E_{exc} (in cm^{-1}).[44] [d] From direct measurements of excited azulene at the given excitation energies E_{exc} (in cm^{-1}).[45]

limiting low-pressure rate constant and the estimated value for the strong collision low-pressure rate constant $k^{SC}_{rec,0}$. Following Troe, $k^{SC}_{rec,0}$ was computed with the equation

$$k^{SC}_{rec,0} = \frac{1}{K_c}[M]Z_{LJ}\frac{\rho_{vib,h}(E_0)kT}{Q_{vib}} \times \exp\left(-\frac{\Delta H^\circ_0 + \Delta E^*_{0Z}}{kT}\right)F_{anh}F_E F_{rot}F_{rot\,int} \quad (20)$$

where $\rho_{vib,h}(E_0)$ is the harmonic density of vibrational states of FSO_2OF at the threshold energy $E_0 \simeq \Delta H^\circ_0$. The F factors take into account corrections for effects of anharmonicity F_{anh}, spread of internal energies F_E, external F_{rot}, and internal rotations $F_{rot\,int}$. The evaluation of these factors is described in detail in ref 15 and 16. The centrifugal barriers used in the calculations of F_{rot} were derived from an effective potential which coupled a Morse interatomic potential with a triatomic centrifugal potential.[16,26,27,37] Because of the lack of information related to the barrier for the FSO_2–OF internal rotation, a value similar to that of CF_3OF, 3.0 kcal mol^{-1},[38,39] was used in the computation of $F_{rot\,int}$. The assumed Lennard-Jones collision parameters for the FSO_2OF are σ = 4.3 Å and ϵ/k = 292 K, while the values tabulated in ref 40 were employed for the bath gases. Q_{vib} is the vibrational partition function of FSO_2OF. Table II summarizes the β_c values derived from our measurements. These results show a typical correlation between β_c and the molecular complexity of bath gases. The exponential and the stepladder models for the transition probabilities have been used for the estimation of $\langle\Delta E\rangle$ from the β_c values derived. These two standard models probably lead, for a given β_c, to the higher and lower bounds of $\langle\Delta E\rangle$, respectively.[41-43] The relationship between β_c and $\langle\Delta E\rangle$ for the exponential model is given by[41]

$$-\langle\Delta E\rangle = \frac{\beta_c}{1-\beta_c^{1/2}}F_E kT \quad (21)$$

while in the stepladder models β_c follows as[42]

$$\beta_c = \left[1 - \exp\left(-\frac{\langle\Delta E\rangle_d}{F_E kT}\right)\right]\tanh\left(\frac{\langle\Delta E\rangle_d}{2F_E kT}\right) \quad (22)$$

The average energy lost in deactivating collisions $\langle\Delta E\rangle_d$ is related to $\langle\Delta E\rangle$ through the following expression

$$-\langle\Delta E\rangle = \langle\Delta E\rangle_d \tanh\left(\frac{\langle E\rangle_d}{2F_E kT}\right) \quad (23)$$

From eq 22 a $\langle\Delta E\rangle_d$ value that fits the β_c is chosen, and then it is transformed to $\langle\Delta E\rangle$ by means of eq 23.

It should be emphasized that the above detailed analysis of the experiments yields values of $\langle\Delta E\rangle$ at energies close to the FSO_2O–F bond dissociation energy. The results of $\langle\Delta E\rangle$ are shown in Table II. All the $\langle\Delta E\rangle$ values estimated with the stepladder model remain smaller than the $\langle\Delta E\rangle$ values obtained with the exponential model. An estimate of the uncertainties of the experiments and of the theoretical analysis leaves an uncertainty of probably a factor of 2 in the calculated $\langle\Delta E\rangle$ values. It appears interesting at this time to compare our $\langle\Delta E\rangle$ values with recent results of directly measured $\langle\Delta E\rangle$ for vibrationally highly excited molecules. Excited CS_2[44] and azulene[45] have been chosen as examples of triatomic and large polyatomic molecules, respectively. $\langle\Delta E\rangle$ values for these molecules at different excitation energies are also given in Table II. It can be seen that the $\langle\Delta E\rangle$ values here calculated fall within the ranges of the results of direct measurements of intermolecular energy transfer. Nevertheless, due to the specificity of the energy transfer and the uncertainties in the $\langle\Delta E\rangle$ values, nothing can be concluded regarding which model for the transition probabilities provides a better interpretation of the energy transfer of this system.

Specific Rate Constants at the Temperature of Experiments. The experimental $k_{rec,\infty}$ and $k_{rec,0}$ values together with the above theoretical analysis allow us to approximately estimate the specific rate constants for decomposition of the energized FSO_2OF adduct at the temperature of the experiments. In terms of the simple mechanism that characterizes the elementary processes involved in a recombination reaction, we have $k_{rec,0} = \beta_c Z_{LJ} k_{rec,\infty}/k(\langle E\rangle,\langle J\rangle)$,[46] where $k(\langle E\rangle,\langle J\rangle)$ is the specific rate constant for a thermal distribution of total energies E and angular momenta J. In this way, from this last relationship the following values were calculated: $k(\langle E\rangle,\langle J\rangle) = 8.7 \times 10^6$, 1.3×10^7, and 1.8×10^7 s^{-1} at temperatures of 298, 339,and 378 K, respectively. These values are significantly higher than those computed for the threshold specific rate constant $k(E=E_0(J=0),J=0) = 8.2 \times 10^4$ s^{-1} which does not depend on details of the potential surface. On the other hand, the particular features of the potential surface determine the opening of available reaction channels and this produces the concomitant sharp increase of $k(\langle E\rangle,\langle J\rangle)$ with excess of energy of FSO_2OF adduct over the threshold value $E - E_0(J=0)$. At low $E - E_0(J=0)$ values (our conditions) the specific rate constants decrease with increasing J.[26,27,47] Besides, the average J value increases with temperature. Therefore, the observed increase of the specific rate constants with temperature is only due to its thermal energy dependence.

Acknowledgment. This research project is supported by the Consejo Nacional de Investigaciones Científicas y Técnicas and the Comisión de Investigaciones Científicas de la Provincia de Buenos Aires. Part of the equipment used in the present work was provided through the Cooperation Agreement between the University of Mainz (W. Germany) and the University of La Plata (Argentina). We also thank the Stiftung Volkswagenwerk for a partnership project with Professor J. Troe.

Registry No. F, 14762-94-8; FSO_3, 15181-47-2; He, 7440-59-7; N_2, 7727-37-9; SF_6, 2551-62-4; CF_4, 75-73-0; FSO_2F, 13536-85-1.

(37) Cobos, C. J. *Int. J. Chem. Kinet.* **1986**, *18*, 459.
(38) Diodati, F. P.; Bartell, L. S. *J. Mol. Struct.* **1971**, *8*, 395.
(39) Buckley, P.; Weber, J. P. *Can. J. Chem.* **1974**, *52*, 942.
(40) Hippler, H.; Troe, J.; Wendelken, H. J. *J. Chem. Phys.* **1983**, *78*, 6709.
(41) Troe, J. *J. Chem. Phys.* **1977**, *66*, 4745.
(42) Snider, N. *J. Phys. Chem.* **1986**, *90*, 4366.
(43) Troe, J. *Z. Phys. Chem. (Munich)* **1987**, *154*, 73.
(44) Heymann, M.; Hippler, H.; Plach, H. J.; Troe, J. *J. Chem. Phys.* **1987**, *87*, 3867.
(45) Hippler, H.; Lindemann, L.; Troe, J. *J. Chem. Phys.* **1985**, *83*, 3906.
(46) Troe, J. In *Physical Chemistry. An Advanced Treatise*; Jost, W., Ed.; Academic: New York, 1975; Vol VIB.
(47) Quack, M.; Troe, J. *Ber. Bunsen-Ges. Phys. Chem.* **1974**, *78*, 240.